A SEPARATE-EFFECT TEST FACILITY FOR CFD-GRADE MEASUREMENTS OF THE RCCS UPPER PLENUM

Thien Nguyen, Victor Petrov and Annalisa Manera
Department of Nuclear Engineering and Radiological Sciences, University of Michigan
2355 Bonisteel Boulevard, Ann Arbor, Michigan, 48109-2104, USA
thienn@umich.edu, petrov@umich.edu, manera@umich.edu.

ABSTRACT

To study important 3D thermal-hydraulics effects affecting the behavior of the air-cooled Reactor Cavity Cooling System (RCCS), a separate-effects scaled facility has been built at the University of Michigan. The experimental facility is a water-based down-scaled model of the air-cooled Natural Convection Shutdown Heat Removal Test Facility (NSTF) upper plenum (Argonne National Laboratory (ANL)), and is aimed at investigating thermal stratification and mixing of multiple risers' (ducts) flows in the RCCS upper plenum. The formation of a stratified layer in the upper plenum is a reactor safety related-issue because it may inhibit the natural circulation process, and interfere with the RCCS performance. In the previous study, preliminary CFD results of the full-scale air-cooled and down-scaled water-cooled RCCS upper plenum have confirmed the scaling analysis.

The current paper experimentally investigates the flow characteristics of constant-density, turbulent risers (jets) vertically discharging into the plenum. Mass flow rates of risers are adjusted to provide the uniform and/or skew velocity profiles at the outlet surfaces of risers representing the practical situations in the reactor cavity. The riser Reynolds number varies from 0.9×10^4 to 1.4×10^4. Particle image velocimetry (PIV) measurements are taken along the central plane of the risers and the central plane of a single riser (parallel to the plenum central plane). From the obtained PIV velocity fields, the flow statistics are computed. Characteristics of the risers' flows inside the plenum are investigated to provide better understanding to the behaviors of the RCCS system.

KEYWORDS
Reactor Cavity Cooling System, riser-jet, hot plenum, PIV, turbulent flow

1. INTRODUCTION

The Reactor Cavity Cooling System (RCCS) is a key safety system for the Next Generation Nuclear Plant (NGNP) gas-cooled thermal reactor and is designed to transfer the core decay heat to the environment under accident situations. The RCCS has been designed for both water-cooled and air-cooled systems, whereas the former is a part of the design of Pebble Bed Modular Reactor (PBMR), and the latter is proposed in the design for the Prismatic Modular Reactor (PMR). The most important feature of the RCCS is a long-term decay heat removal capability which is very useful for other high-temperature reactor designs as well. Recent RCCS designs consist of pipes (ducts) that are located inside the reactor cavity and face the reactor pressure vessel (RPV). Fluid flowing inside the RCCS pipes through natural circulation removes the RPV heat by radiation and convection. The RCCS systems operate in a passive mode and are able to remove the core decay heat without the need for off-site power or operator action.

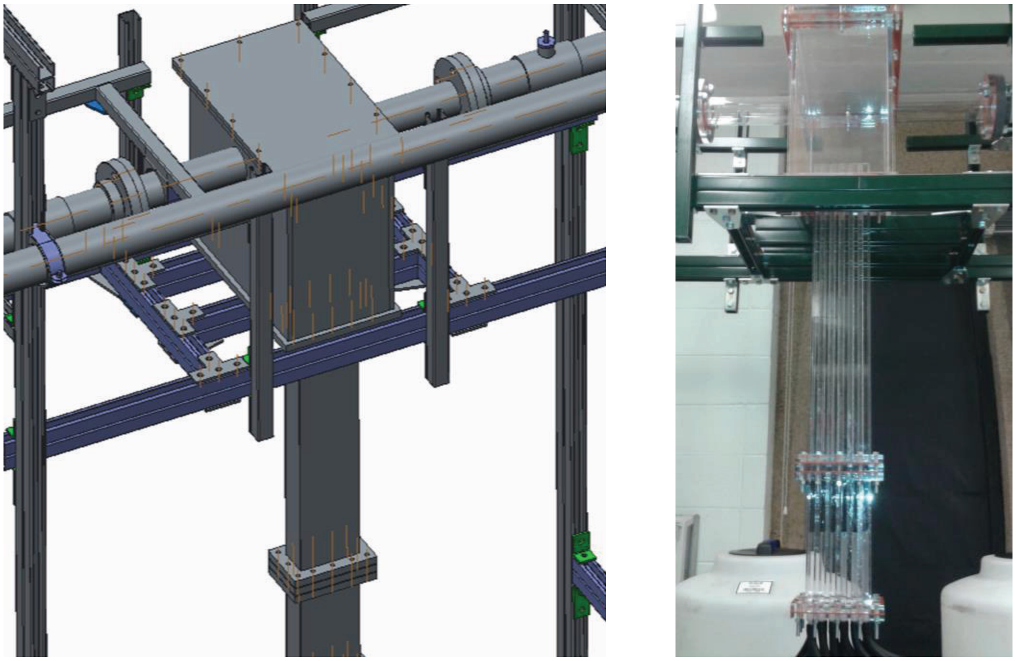

Figure 1. CAD design (left) and photo (right) of the separate-effects scaled facility.

The Natural Convection Shutdown Heat Removal Test Facility (NSTF) [1-3] has been built at the Argonne National Laboratory (ANL) to provide a large scale simulation of the air-cooled RCCS. Experimental results on this facility have provided supports for the design and analysis of the RCCS system. However, the NTSF instrumentations, while suitable for validation of system codes, do not always provide the necessary resolution for validation of Computational Fluid Dynamics models. In addition, visualization and understanding of local relevant 3D effects might be difficult.

To study important 3D thermal-hydraulics effects affecting the behavior of the air-cooled RCCS and complement the experimental and validation activities done at the ANL, a separate-effects scaled facility has been built at the University of Michigan (UofM), and aimed at the simulation of the upper plenum of the air-cooled RCCS. Our objective is to both gain physical insight in the thermal-hydraulic phenomena taking place in the RCCS upper plenum, so that the predictive capabilities of CFD codes can be assessed and further improved. The experimental facility built at the University of Michigan is a water-based down-scaled model of the air-cooled NTSF upper plenum, and is aimed at addressing thermal stratification and mixing of multiple risers' (ducts) flows. The formation of a stratified layer in the upper plenum is a reactor safety related-issue because it may inhibit the natural circulation process, and interfere with the RCCS performance. Preliminary CFD results of the full-scale air-cooled and down-scaled water-cooled RCCS upper plenum have confirmed the scaling analysis [4], which was carried out to facilitate the scaled-model to mimic the flow characteristics of the riser ducts' flows when entering the hot plenum. In other words, the rising of risers' flows to the upper plenum due to natural convection in the full-scale air-cooled RCCS is imitated in the scaled water-cooled RCCS as forced convection by using water pump. In such circumstances, the down-scaled water-cooled RCCS upper plenum have taken into account the measured and observed parameters, such as the Reynolds number, Froude number, momentum and buoyant energy, from the full-scaled air-cooled RCCC as the input, initial and boundary conditions in the scaled-model, such as the Reynolds number, Froude number, momentum and buoyant energy. These considerations simplified the separate-effects scaled facility into a case of vertical jets discharging into the plenum volume. The operating fluid of the scaled-model is water, whose density can be adjusted by adding sugar and/or alcohol. In this way, the heating of the working fluid is avoided, eliminating the uncertainties associated with heat losses. Problems with the thermal stratification in the full-scale RCCS can be investigated in the separate-effects scaled facility by discharging the risers' flows into the plenum which is stratified in advance with the denser water-based fluid.

As the first stage of our research objective, this paper experimentally investigates the flow characteristics of same density, turbulent risers (jets) vertically discharging into the plenum. Mass flow rates of risers are adjusted to provide the uniform and/or skew velocity profiles at the outlet surfaces of risers representing the practical situations in the reactor cavity. The riser flow Reynolds number varies from $Re_r = 0.9\times10^4$ to 1.4×10^4. Preliminary investigations are executed by performing particle image velocimetry (PIV) measurements along the central plane of the risers and the central plane of the plenum. From the obtained PIV velocity fields, the flow statistics are computed and discussed. Characteristics of the risers' flows inside the plenum are investigated to provide better understanding to the behaviors of the RCCS system.

2. SEPARATE-EFFECTS SCALED FACILITY AND EXPERIMENTAL SETUP

In this section, details on the separate-effects scaled facility and an experimental setup of PIV measurements are presented.

2.1. Separate-Effects Scaled Facility

In [4], CFD results calculated from the RCCS full-scale model and the scaled-model have confirmed the soundness of the scaling analysis where measured or observed parameters, such as the Reynolds number, Froude number, momentum and buoyant energy, from the RCCS full-scale prototype are taken into account as the input, initial and boundary conditions in the scaled-model. From this scaling analysis study, geometrical dimensions of the separate-effects scaled facility, such as riser width, riser length, distance between risers, distance between risers and plenum walls are downscaled from those of the ANL facility by a factor $f_{scale} = 4$. To reduce the complexity of the experimental facility, the number of risers is reduced from 12 to 6, similarly to the air-cooled scaled facility built at the University of Wisconsin. The effect of having 6 risers instead of 12 has been analyzed by means of CFD simulations and it has been found that the flow patterns and dominant flow structures calculated from facility with 6 and 12 risers are similar.

Figure 1 illustrates the 3D CAD design and a photo of the scaled facility. The separate-effects scaled facility was fabricated in transparent acrylics to allow access for optical laser measurements. The upper plenum has the inner dimensions of length × width × height = 470.6 × 249.3 × 462 (mm^3) and two exhaust pipes with an inner diameter of 76.2 (mm). A pack of six risers, whose distance between neighbouring risers is $S_r = 12.7$ (mm), was attached with an intrusion of 63.5 (mm) to the bottom of the plenum. The working fluid of the facility, i.e. water, was stored in two tanks of 400 liters and one tank of 2000 liters. In the present experiments, tap water was supplied at room temperature by three centrifugal pumps and guided into the risers, where each riser has $D_1 \times D_2 = 12.7 \times 63.5$ (mm^2) cross section. The water flow was driven through a conditioning section with honeycomb grids and long channels to obtain a uniform water jet flow and to minimize the turbulence level. The axial length L_{riser} of the risers is 800 (mm) yielding the ratio $L_{riser}/D_r = 38.1$ (D_r is the hydraulic diameter of the riser), which is sufficiently long for the flow to reach a fully developed state. Flow rates of six risers were regulated by gate valves and accurately measured by turbine flow meters (Blancett 1100). In the current facility, two risers were connected to one pump controlled by a variable frequency drive. In this paper, flow rates in each risers varied from 0.35 to 0.53 (l/s) yielding the mean velocities in the risers from 0.43 to 0.66 (m/s). The riser Reynolds numbers, which were based on the riser velocity U_j, the riser hydraulics diameter D_r, and the kinematic viscosity ν, were 0.9×10^4 to 1.4×10^4. The x, y and z coordinates, respectively, represent the horizontal, vertical and spanwise directions. The origin of the coordinate system is at the bottom left corner of the plenum. The velocity components corresponding to the x, y and z directions are U, V and W for the time-averaged velocity and u', v' and w' for the fluctuating velocity, respectively.

2.2. PIV experimental setup

Figure 2 shows the 2D2C PIV experimental setup. The flow characteristics in the region 1, formed by the middle plane of the risers (an *yz*-parallel plane), and the region 2, formed by the middle plane of a single riser nearest to the exhaust (an *xz*-parallel plane), were investigated by performing PIV measurements. The PIV system consisted of a high repetition rate Nd:YLF, double cavity, dual head laser (Photonics Industries) with an articulated light arm, two digital CMOS Phantom M340 cameras, a high speed controller and a computer. Each laser beam was capable of 35 mJ/pulse at the wavelength of 527 nm. These beams were adjusted by beam combination optics to form a 2-mm-thick laser sheet for the PIV measurements. The high-speed Phantom M340 cameras with a full resolution of 2560 × 1600 pixels, a pixel size of 10 × 10 μm^2 and 12-bit depth captured PIV images and instantly stored them to the 12GB high-speed internal RAM. The high speed controller (LaVision model 1108075) controlled the synchronization between the lasers and the cameras. Seeding particles were hollow glass spheres with a mean diameter of 10 µm and were mixed in the storage tank. During the experiments, the water flow was driven from the storage tank, pumped into the plenum via the risers, and returned to the tank. The flow therefore was circulated and that tracers were present in the risers and the plenum.

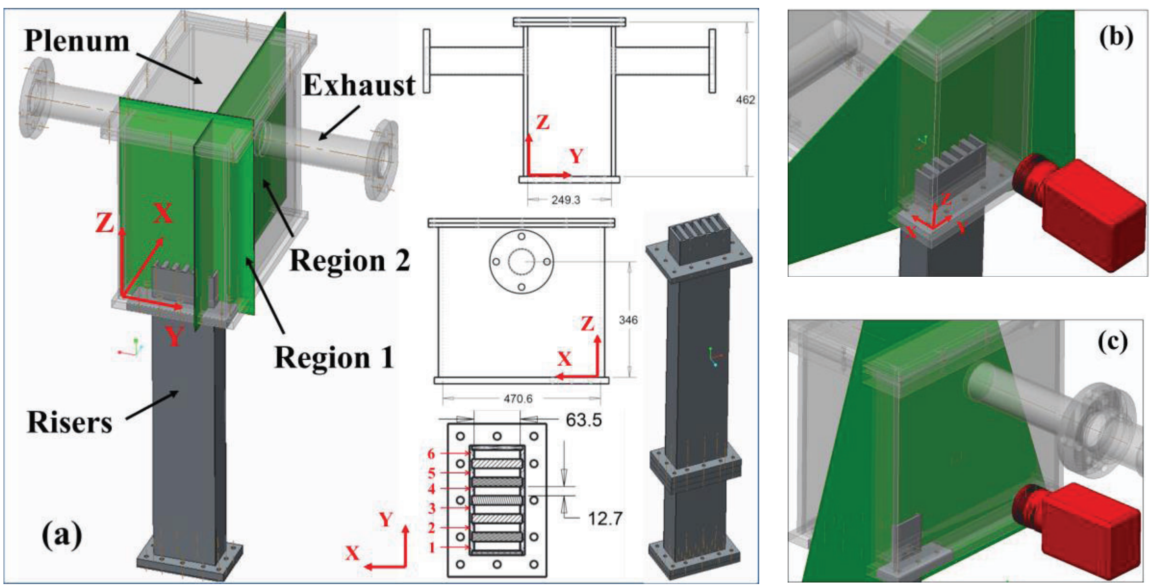

Figure 2. Drawings and dimensions of the plenum and risers in the scaled facility *(a)*, PIV experimental setups for region 1 *(b)* and region 2 *(c)*.

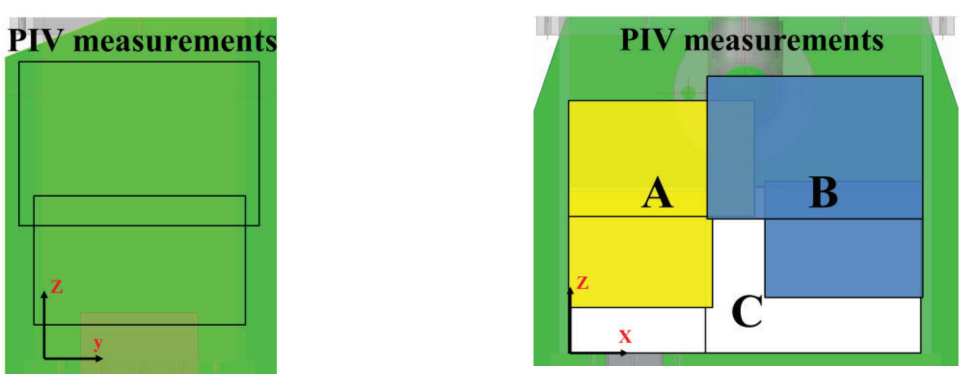

Figure 3. Flow areas covered in the PIV measurements at the region 1 *(left)* and region 2 *(right)*.

In the 2D2C PIV measurements, fluid images in the *yz* plane with z/D_1 ranging from 0 to 31 for the region 1, and fluid images in the *xz* plane with z/D_1 ranging from 0 to 28 for the region 2, were taken. At each of the region (1 and 2), two cameras simultaneously recorded the particle images. Fields of views of two cameras were then adjoined to enlarge the measured area (see Figure 3). A sequence of 2013 images (2560 × 1600 pixels) in a single-frame mode was recorded during each run with a sampling rate ranging from 500 Hz to 700 Hz depending on the riser velocity. Within these frame rates, inter-pulse time delays, denoted by Δt, varied from 1428 μs to 2000 μs, yielding maximum particle displacements of 10 pixels. The total recording time covered from 136 to 149 eddy turn-over times where an eddy size of D_1 was a considerable large-scale structure of the flow, and an eddy turn-over time was defined by D_1/U_j. Given that the recorded times were long enough; results computed from the captured flow images could statistically represent the characteristics of the flow.

Image acquisition and image processing were done with DaVis 8.2 software by LaVision Gmbh. The PIV experimental images were processed by an advanced image deformation multi-pass multi-grid PIV cross-correlation and a 50% window overlap. For both sets of measurements, the first pass started with an interrogation window of 64 × 64 pixels and the final pass ended with an interrogation of 32 × 32 pixels. Vectors were calculated from the correlation map with a Gaussian peak fit for sub-pixel accuracy [5]. Inside each pass, statistical validations were done to identify and replace erroneous vectors. A median filter [6] was applied and standard deviations of the neighboring vectors were used to filter spurious vectors. The grid spacing in the 2D2C PIV velocity vectors varied from 1.84 (mm) to 2.09 (mm) for regions 1 and 2, i.e. $0.14D_1$ and $0.16D_1$. The percentage of bad vectors for the PIV measurements approximated from 2% to 5%, respectively.

3. RESULTS OBTAINED BY THE PIV MEASUREMENTS

This section presents the flow field results obtained from the PIV measurements. Experimental flow statistics calculated at the central plane of the risers (region 1) and at the central plane of the single riser 1 (region 2) are presented.

3.1. PIV results obtained from the central yz-plane of the risers

In this configuration, experimental images were taken at the central plane of risers and the water flow was discharged from different risers with various flow rates.

Figure 4 shows contours of the time-averaged vertical velocity from the riser 3 and 4 at the riser Reynolds Re_r = 0.9×10^4 and 1.4×10^4. Snapshots of instantaneous velocity vectors and vorticity colormaps are displayed to reveal the overall flow dynamics of the risers discharged into the plenum. In this flow configuration, fluid flow discharged from the two risers can be similarly considered as the two parallel plane jets/risers with a jet separation ratio, i.e. ratio of the jet axis distance and D_1, of 2, and an aspect ratio of 5. The vertical *z*-axis of the plenum is the plane of symmetry bisecting the distance between two risers. Details on the studies of two parallel jets can be reviewed in [7-13]. These authors have discussed that for the two parallel risers, three flow regions can be identified. The converging zone is the region from the riser exit to the merging point where the inner shear layers of the risers merge. A low-pressure zone close to the risers' wall and the inner shear layers is created by high entrainment rates in this region. This causes the individual riser flow to curve towards each other. The merging point is defined as the streamwise location where the mean streamwise velocity decays to zero [12]. Downstream of the merging point, two risers continue to interact with each other up the combined point, defined at the location where streamwise velocity reaches its maximum. Further downstream, the two risers merge to form a single flow pattern. However, compared to the above studies with non-confined parallel jets, flow patterns of the parallel risers in the current experimental configuration were expected to be more complicated because the risers discharged into the plenum with the confined walls and two exhausts.

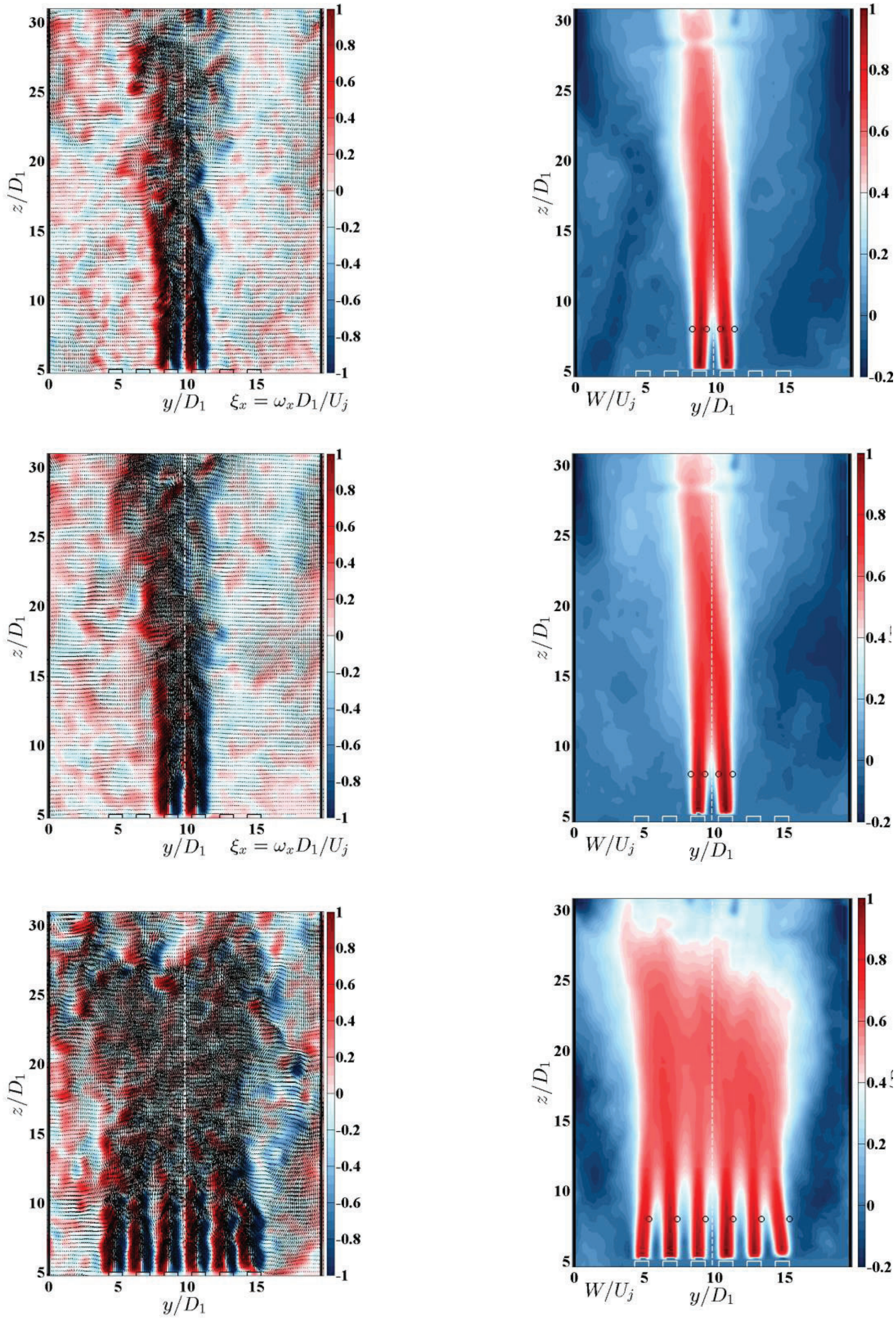

Figure 4. PIV results obtained from the central plane of two risers (3 and 4) for Re_r = 0.9×10^4 (*top*) and 1.4×10^4 (*middle*), and of six risers for Re_r = 1.4×10^4 (*bottom*). Instantaneous velocity and vorticity (*left*) and time-averaged vertical velocity (*right*). Velocity and vorticity are normalized by the riser velocity and eddy-turn over time (D_1/U_j), respectively.

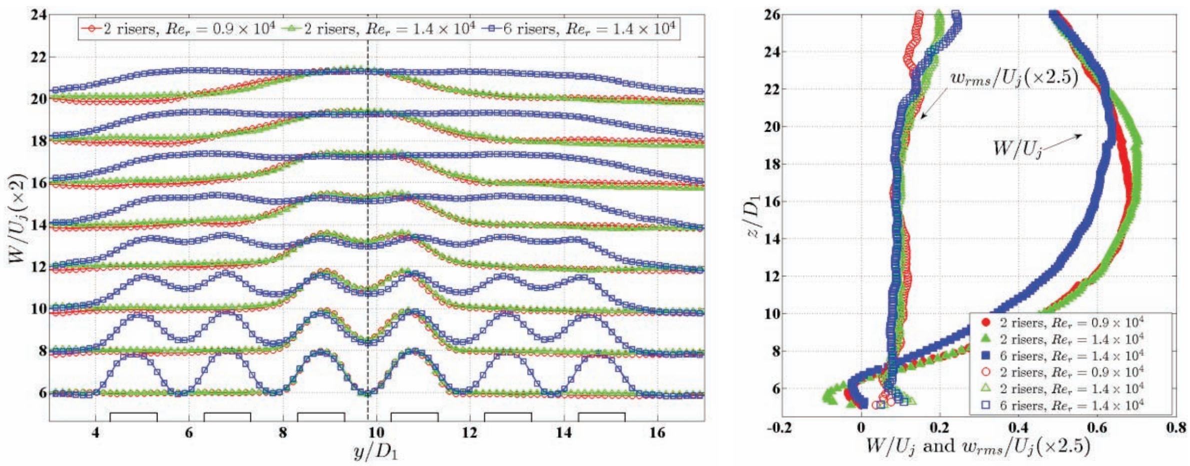

Figure 5. Time-averaged vertical velocity profiles at several vertical (streamwise) distance from the riser exits obtained by the PIV measurements at the *yz*-plane (*left*), time-averaged vertical velocity and root-mean-square fluctuating vertical velocity along the riser centerline (*right*).

It is noted that because the riser has an aspect ratio of 5, the discharged fluid flow from the riser exhibits the three-dimensional structures instead of the quasi-three dimensional patterns commonly found in many previous studies on rectangular jets with the aspect ratio larger than 20.
It can be seen from the Figure 4 that after being discharged into the plenum, the risers' flows started to interact with each other along the vertical axis. The riser moved towards the symmetry plane due to a mutual flow entrainment between them [13]. Time-averaged vertical velocity profiles at several streamwise distance from the riser exits in Figure 5 for the cases of two risers (3 and 4) at the Reynolds numbers Re_r = 0.9×10^4 and 1.4×10^4 are well overlapped indicating that the Reynolds increase yields insignificant effect to the flow. Vortices were generated by the inner shear layers, rolled upward and appeared to combine or counterbalance each other. On the other hand, vortices created by the outer shear layers were convected by the riser flow further in the vertical direction until they impinged to the plenum top wall, deflect to the plenum corners. It can be seen from the instantaneous velocity vectors and the contours of the mean vertical velocity that there are downward flows on the vertical walls. Such flow patterns were imprints of the secondary recirculation flow appeared at the top corners above the risers while the primary recirculation flow was present in the central volume of the plenum observed in the *xz*-plane PIV measurements. The primary and secondary recirculation flows will be discussed in the next section.

Contours of mean vertical velocity in Figure 4 indicate that after merging into the single pattern, the flow started to deviate to the left side of the symmetry plane. The asymmetrical flow of two parallel jets was also found in [10] where the authors have reported that the loci of the maximum local mean streamwise velocity and the convecting of the inner and outer vertical structures are nearly parallel to the symmetry plane until $7.5D_j$. In the current configuration, there are several factors that may cause asymmetries in the risers' flow, such as the difference of risers' flow rates, the confinement, the presence of the exhausts, and the pressure difference between two flow exits via the exhausts. Maximum difference among the flow rates of the risers' flows was found to be less than 3% during the PIV experiments. The effects of the plenum confinement (i.e. the top, front and back walls), two exhaust pipes and the pressure difference between the outflows via the exhausts were probably concerned because those have driven the risers flow in the positive x-direction (perpendicular to the PIV measurement plane). The driven force yielded stronger effects to the vortical structures operating in the positive *x*-direction and that caused the combined flow curved toward one side.

The flow patterns and contours of the time-averaged vertical velocity for the case of six risers discharged into the plenum at $Re_r = 0.9 \times 10^4$ are displayed in Figure 4. The instantaneous velocity vectors and vorticity colormap show that the mutual risers' interactions, vortex generation by the shear layers, merging and counterbalancing of vortices, which have been discussed above, were strongly enhanced by the presence of discharged flow from six risers. This figure illustrates a high population of spanwise (*x*-direction) vortices at the size of riser width D_1 and a high degree of three-dimensionality of the flow. These vortical structures were also observed near the vertical wall resulting to the downward flows in those flow regions. Moreover, the downward flows increased their penetrations in the negative z-direction and interacted with the two outward risers' flows, i.e. riser 1 and 6. These interactions yielded the two risers' flows curved towards the symmetry plane as can be seen in the contour of mean velocity. The time-averaged vertical velocity profiles at several vertical distances overplotted in Figure 5 have confirmed these interactions. The velocity profiles at $z/D_1 = 6$ and each individual profile of six risers are identical to those from the case of two risers (3 and 4). The overall shapes of the two outward velocity profiles, i.e. locations of the local maximum and minimum peaks, have changed from the location $z/D_1 = 10$ indicating these two risers' flows curvature towards the symmetry plane. The plots of velocity profiles also show that all the risers' flows start to form a single flow pattern from a certain vertical location, around $z/D_1 = 15$ to 16, where all the velocity peaks are nearly flat. It is interesting to find that the merging points, where $W/U_{j\text{-centerline}} = 0$, determined for the cases of two risers and six risers discharged into the plenum were nearly identical, i.e. ranging from $6.5D_1$ to $6.6D_1$. Downstream of the merging point, the risers' flows merged at the combined point of $z/D_1 = 15$ for the case of two risers and $Re_r = 0.9 \times 10^4$, while the combined point of $z/D_1 = 19.2$ was found for the case of two and six risers and $Re_r = 1.4 \times 10^4$. The profiles of the r.m.s fluctuating vertical velocity yielded peaks inside the merging region, which was similarly found in [13], and gradually increased from the combined point. On the other hand, vortices created by the outer shear layers were convected by the riser flow further in the vertical direction until they impinged to the plenum top wall, deflected to the plenum corners. It can be observed from the instantaneous velocity vectors and the contours of the mean vertical velocity that there are downward flows on the vertical side walls.

Figure 6 shows the power spectra of the fluctuating velocity v' (y-direction) versus the Strouhal number, which is defined by $St = fD_1/U_j$, at points 1-4 for the riser Reynolds $Re_r = 0.9 \times 10^4$ and 1.4×10^4. These points were located in the outer and inner shear layers of two risers (see points from left to right in Figure 4) and have a distance of $3D_1$ from the riser exit. In the spectral distribution of velocity fluctuations at the inner shear layer, i.e. $y/D_1 = 9.135$ and 10.135, and $z/D_1 = 8$, a dominant Strouhal number St=0.27 was found that is close to the value of $St = 0.273$ obtained in [14] for the turbulent plane jet at $Re = 6000$. On the other hand, spectral distributions obtained at the points located in the outer shear layer, i.e. $y/D_1 = 8.135$ and 11.135, showed different dominant frequencies at two Reynolds numbers. The wide ranges of frequency detected in the spectral distributions can be explained by the appearance and the penetration of the surrounding vortices into the riser core flows. These vortices returned to the core flows after impinged to the plenum top wall, or those from the downward flows at the plenum vertical walls, and interacted with the vortices that were just generated from the shear layers.

Figure 7 displays the spectral distributions of fluctuating velocity v' (*y*-direction) versus the Strouhal number at points 1-6 (see points from left to right in Figure 4) located in the inner shear layers of six risers for the riser Reynolds numbers $Re_r = 0.9 \times 10^4$ and 1.4×10^4. Similar to the detected dominant frequency of points located in the inner shear layers of two risers, the Strouhal numbers of $St = 0.25$ and 0.27 were seen in the spectral distributions of the points in the inner shear layers of six risers. However, these Strouhal numbers did not always correspond to the most dominant frequency, i.e. points 2 and 5, indicating that the flow fields contained many vortices generated from the six risers and their interactions. Several peaks in the power spectral of point 6, which was located in the outer shear layer, show the similar flow phenomenon of the penetration of surrounding vortices into the riser flow.

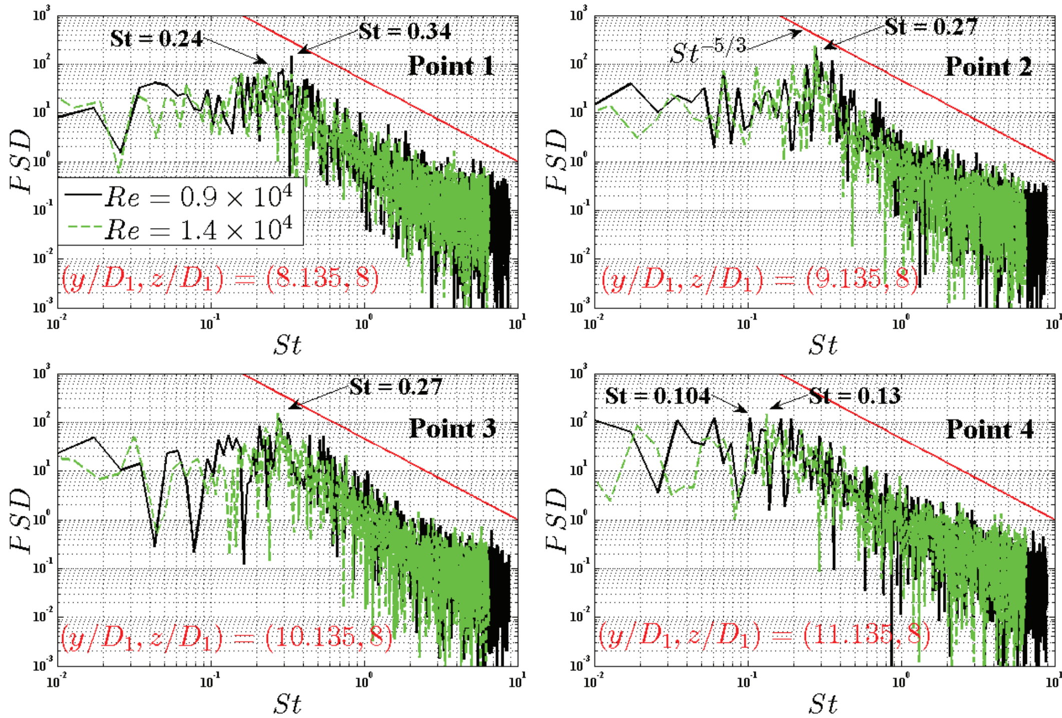

Figure 6. Power spectra of fluctuating velocity *v′* (y-direction) at points 1-4 (points from left to right in Figure 4) located in the shear layers obtained by PIV measurements in the central plane of two risers (3 and 4) for Re_r = 0.9×10^4 (solid black) and 1.4×10^4 (dash green).

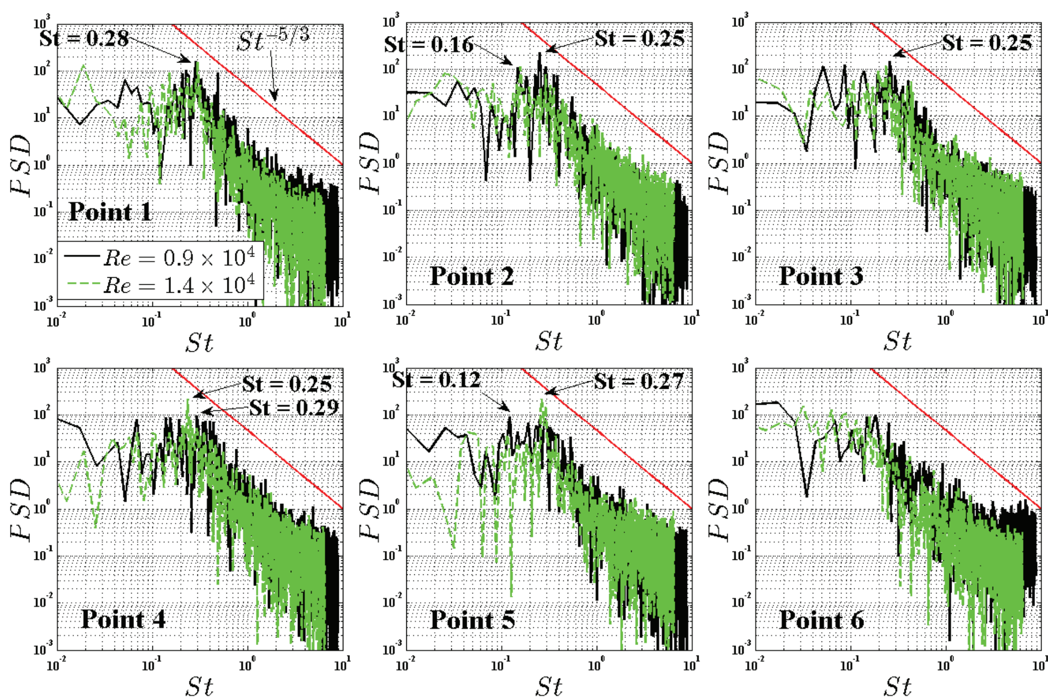

Figure 7. Power spectra of fluctuating velocity *v′* (y-direction) at points 1-6 (points from left to right in Figure 4) located in the shear layers obtained by PIV measurements in the central plane of six risers for Re_r = 0.9×10^4 (solid) and 1.4×10^4 (dash).

3.2. PIV results obtained from the central xz-plane of the single riser

In this configuration, images of fluid flow in the central plane of the single riser, i.e. riser 1, were taken while the PIV cameras were arranged and placed at several positions. Figure 3 (*right*) shows the areas of the fluid flow in the region 2 measured by the PIV measurements. In these PIV measurements, images of three fluid areas in the *xz*-plane, i.e. **A**, **B** and C, were separately captured. For each area, two cameras recorded the experimental images and the obtained velocity vector fields were then merged to provide larger fields of views. Coordinates of the bottom left and top right corners of the measured areas by two cameras were given here. The area **A** covered (x/D_1, z/D_1) from (0, 5) to (13.8, 14.9), and from (0, 13.1) to (19.1, 25.2). The area **B** ranged from (12.2, 13) to (36.2, 28.3), and from (20.9, 5.8) to (36.2, 15). The area **C** ranged from (0, 0) to (25.6, 16.1), and from (11.8, 0) to (36, 15.5).

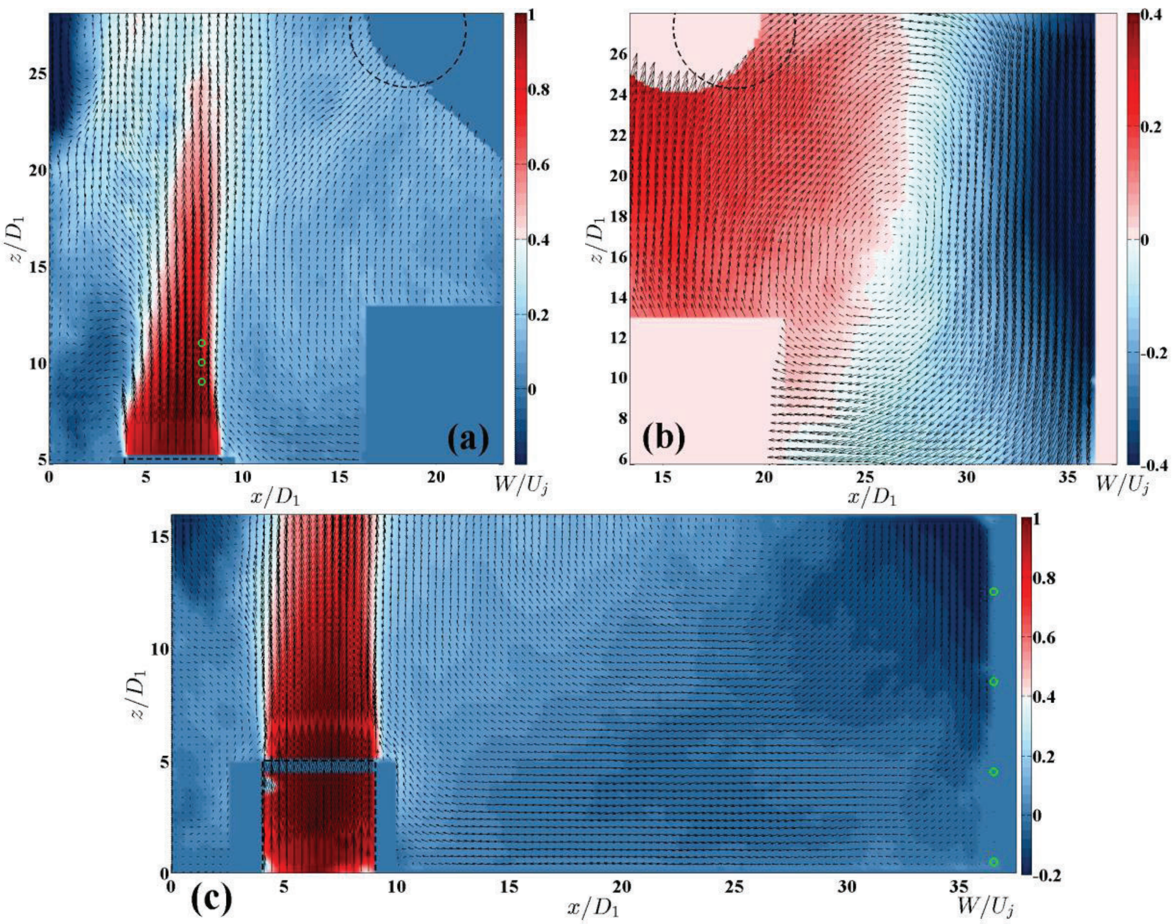

Figure 8. Time-averaged velocity magnitude obtained by PIV measurements in the central plane of the single riser. PIV results and at the area A (a), B (b) and C (c) for $Re_r = 0.9\times10^4$.

Figure 8 and Figure 9 show the mean velocity vectors and the contours of the vertical velocity component that were obtained from the PIV measurements in the region 1 and at the area **A, B** and **C** for the riser Reynolds numbers for $Re_r = 0.9\times10^4$ and 1.4×10^4, respectively. The velocity vectors were normalized by the riser velocity while the horizontal and vertical axes were normalized by the jet width D_1.

Effects of an increase in the riser Reynolds number can be seen from the contours of the PIV measurements at the area **A** where the riser penetrated further into the plenum and its flow curvature was

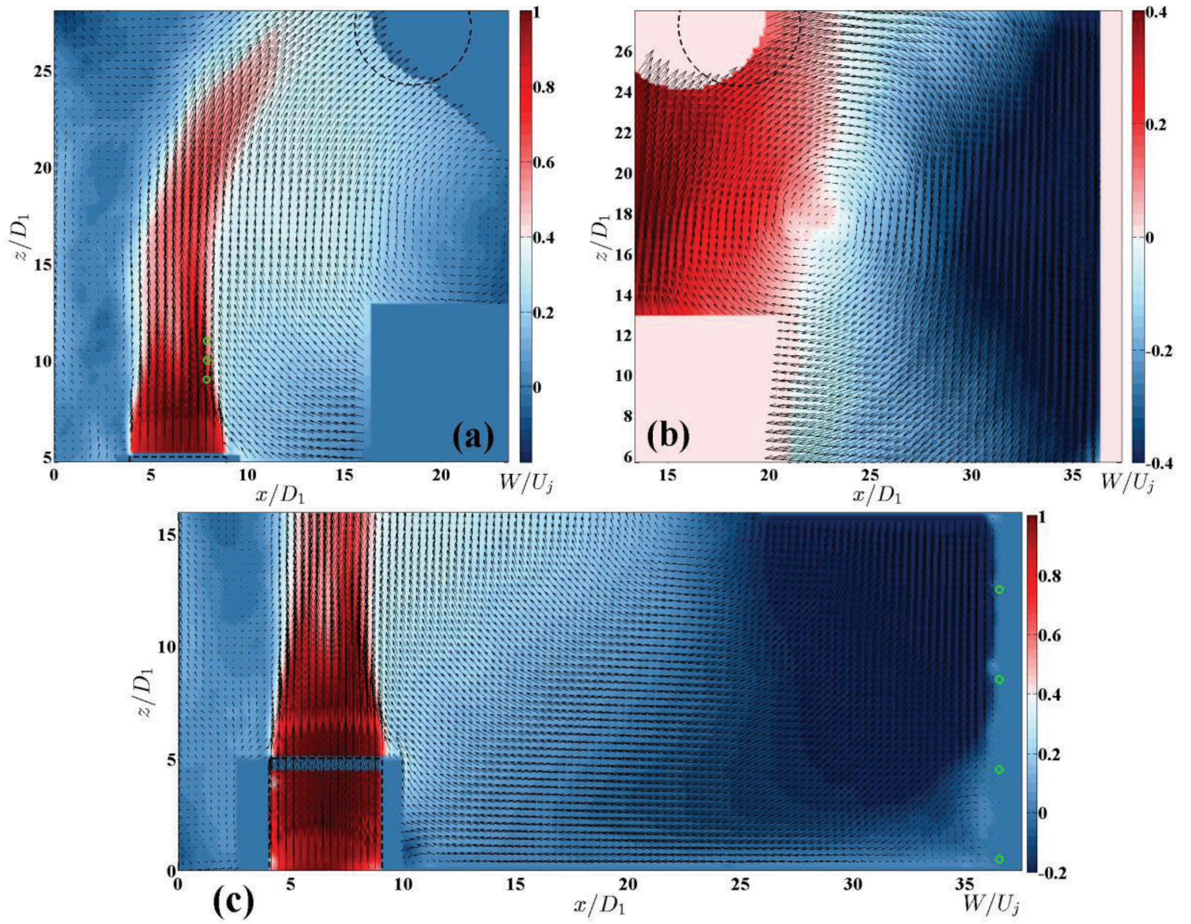

Figure 9. Time-averaged velocity magnitude obtained by PIV measurements in the central plane of the single riser. PIV results and at the area A (a), B (b) and C (c) for Re_r = 1.4×10^4.

strongly curved towards the exhaust at Re_r = 1.4×10^4. At both Reynolds numbers, the secondary recirculation flows were observed at the top left corner of the plenum. The recirculation region created by the riser flow at Re_r = 1.4×10^4 extended wider in the x-direction because of the riser's greater penetration and its impingement to the plenum top wall. The downward flows found in the PIV experiments at the region 1 (see section 3.1) were caused by the presence of the secondary recirculation flows in the area **A**. Moreover, the presence of the primary recirculation can be seen in the central volume of the plenum and its region was separated with the secondary recirculation by the riser's bulk flow. The velocity vectors and colour contours (rescaled to ±$0.4W/U_j$ for better visualizations) obtained by the PIV measurements in the area **B** revealed clearer views of the primary recirculation flows. The increase of riser Reynolds numbers has shifted the center of the primary recirculation region from (x/D_1, z/D_1) = (25.8, 16.1) for Re_r = 0.9×10^4 to (x/D_1, z/D_1) = (23, 17.5) for Re_r = 1.4×10^4. Ratios of the vertical velocity component magnitude to the riser velocity and the width of the return flow region near the vertical right wall also increased in associated with the increase of Reynolds number. The return flow was formed near the vertical wall, directed in the negative *z*-direction and was rather similar to the wall jet flow until it reached the plenum bottom corner. Results obtained from the PIV measurements at the area **C** partially show the lower regions of the primary recirculation and the bottom corners of the plenum. No recirculation region was visible at the bottom corners at Re_r = 0.9×10^4, while two recirculation regions, one with the size $3D_1$ at the bottom right and one with the size of $3D_1$ at the bottom left, were clearly observed at Re_r = 1.4×104. The expansion of the primary recirculation region in size and magnitude probably affected the width of riser flow after the riser exit. At Re_r = 1.4×104, the primary recirculation penetrated deeper into the riser core compared to that effect caused by the secondary recirculation. Both penetrations of the primary and secondary recirculation flows thinned the riser width and yielded two local peaks inside the riser flow.

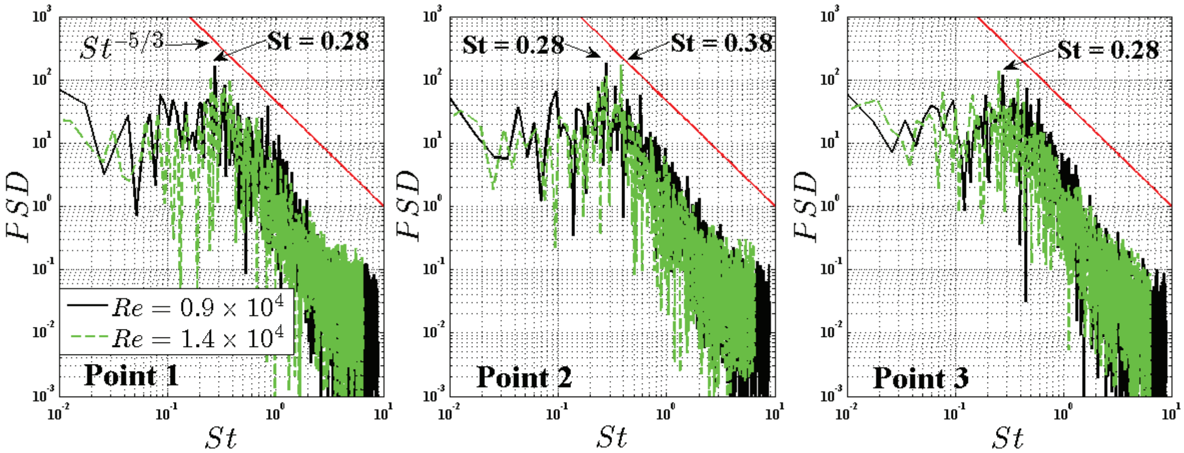

Figure 10. Power spectra of fluctuating velocity *u′* (*x*-direction) at points 1-3 (points from bottom to top in Figure 8, area A) located in the shear layers obtained by PIV measurements in the central plane of the single riser for $Re_r = 0.9\times10^4$ (solid) and 1.4×10^4 (dash).

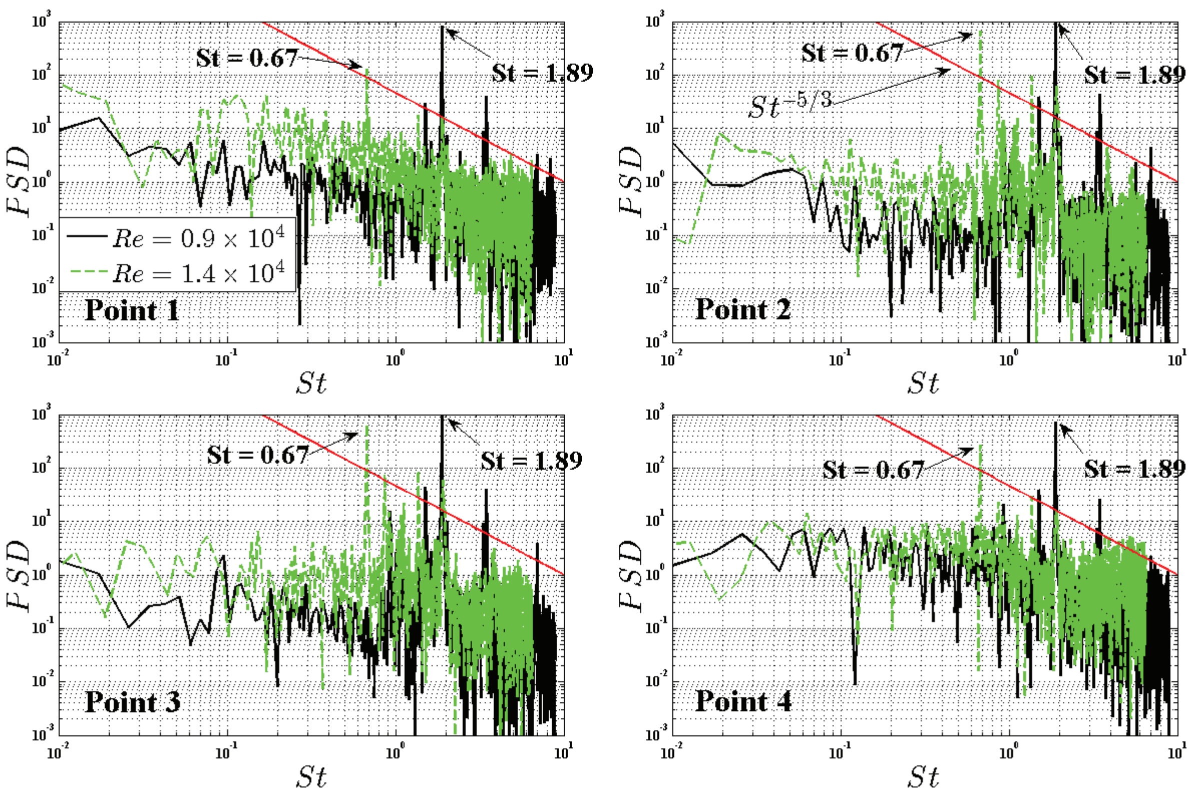

Figure 11. Power spectra of fluctuating velocity *u′* (x-direction) at points 1-4 (points from bottom to top in Figure 8, area C) located near the plenum vertical wall obtained by PIV measurements in the riser central plane for $Re_r = 0.9\times10^4$ (solid) and 1.4×10^4 (dash).

In Figure 10, spectral distributions of the fluctuating velocity u' (x-direction) at three points obtained by the PIV measurements at the area **A** for the riser Reynolds numbers of 0.9×10^4 and 1.4×10^4 are shown. These three points (see points from bottom to top in Figure 8) were located in the shear layer of the single riser. A dominant Strouhal number St = 0.28 is observed that is consistent to the dominant Strouhal number found from the spectral distributions of the other points located in the inner shear layers of the risers' flows. It is mentioned above that due to the riser aspect ratio of 5, the risers' flows generate high populations of vortices from the shear layers formed on both dimensions D_1 and D_2. The single dominant Strouhal number found on several points located in the shear layers indicated that the vortex generation mechanism is governed by the same dominant frequency. However, in the region characterized by interactions of generated vortices and those returned after impinging to the confinement wall, the wide range of frequency was observed as in the outer shear layers of the risers.

Figure 11 shows spectral distributions of the fluctuating velocity u' (x-direction) at four points, which were located near the plenum vertical wall, obtained by the PIV measurements at the area **C** for Re_r = 0.9×10^4 and 1.4×10^4. It is interesting to find that in this region, the dominant Strouhal numbers of St = 1.89 and 0.67 were detected for the riser Reynolds number of 0.9×10^4 and 1.4×10^4, respectively. As shown in the PIV mean velocity vectors, the return flow formed like the wall jet flow near the vertical wall and directed in the negative z-direction. However, vortical structures in this region originate from those generated by the risers; their sizes are comparable to the riser width D_1. Populations and rolling motions of the large-scale structures strongly depend on the Re_r when more vortices are generated from the riser exits and travelled further into the plenum volume, impinged to the wall. These have yielded the difference in the Strouhal numbers found in this are for the two Reynolds numbers.

4. CONCLUSIONS

In this paper, we have presented the separate-effects scaled facility built at the University of Michigan to study the thermal-hydraulics effects affecting the behavior of the upper plenum of the air-cooled RCCS. The experimental facility is a water-based, down-scaled set-up of the ANL NSTF upper plenum. Six risers discharged the water flow into the plenum volume and the riser Reynolds numbers ranged from 0.9×10^4 to 1.4×10^4. Preliminary investigations have been done to study the flow characteristics of the risers, their mutual interactions and the flow patterns in the plenum by performing PIV measurements. A first set of PIV measurements has been performed in the central plane of the risers to reveal the risers flows and their interactions while the second set has been done in the central plane of the single riser and at several regions to study the flow patterns inside the plenum volume.

In the first set of PIV measurements, the PIV snapshots of instantaneous and time-averaged velocity fields have revealed the flow dynamics of the risers discharged into the plenum that were characterized at several regions. The fluid flow near the riser areas can be identified by the converging region, the merging region, the combined region and the near plenum wall region. The former three regions were the characteristics of the parallel jets and the dominant Strouhal numbers of St = 0.25 to 0.29 have been observed from the spectral distributions. The latter region was created due to the interactions of the vortices generated from the risers' shear layers and the plenum wall. It is seen that with an increase of Reynolds number, the mutual risers' interactions, vortex generation were enhanced with the high population of vortices in the observed region, downward flows near the vertical walls and the deeper penetrations of the return flows into the riser core flows.
In the second set of PIV measurements, it is seen that the riser flow penetrates further into the plenum and its flow curvature was strongly curved towards the exhaust when the riser Reynolds number increased. Inside the plenum volume, the primary recirculation flow was formed by the interactions of the risers' flows and the plenum top wall, further vertical wall and bottom wall while the secondary recirculation region was created by the risers interacting with the plenum top wall, closer vertical wall and bottom wall. Size of the primary recirculation zone increased and its center location was shifted in associated with the

increase of Reynolds number. In such situation, the primary recirculation region expanded and penetrated further into the riser core compared to the effect from the secondary recirculation that thinned the width of the riser flow. In addition, two sub-region recirculation flows have been found at the bottom corners of the plenum for the $Re_r = 1.4\times10^4$. Near the further vertical wall, the return flow was formed by the vortical structures rolling in the negative z-direction. The Strouhal numbers in this region have decreased from $St = 1.89$ to 0.67 with the increase of Reynolds numbers from $Re_r = 0.9\times10^4$ to 1.4×10^4.

Further investigations will be performed with variable density fluids in the risers discharged into the plenum with asymmetrical profiles. Moreover, measurements will be done by applying wire-mesh sensors [15] manufactured at the University of Michigan, ECMF laboratory, and by combining PLIF and PIV measurements to acquire high resolution measurements of the concentration and velocity fields.

REFERENCES

1. R. V. Vilim and E. E. Feldman, "Scalability of the Natural Convection Shutdown Heat Removal Test Facility (NSTF) Data to VHTR/NGNP RCCS Designs", *ANL-GenIV-049*, 2005.
2. C. Tzanos, "CFD Analysis for the Applicability of the Natural Convection Shutdown Heat Removal test Facility (NSTF) for the simulation of the VHTR RCCS", *ANL-GenIV-055*, 2005.
3. M. T. Farmer, et. al., "Natural Convection Shutdown Heat Removal Test Facility (NSTF) Evaluation for Generating Additional Reactor Cavity Cooling System (RCCS) Data", *ANL-GenIV-058*, 2005.
4. T. Nguyen, V. Petrov, A. Manera, "Design of a scaled experimental facility for the NGNP Reactor Cavity Cooling System", *American Nuclear Society 2014 Winter Meeting and Technology Expo*, Anaheim, California, 2014.
5. Raffel M., Willert C., Wereley S., Kompenhans J., *Particle image velocimetry: a practical guide*. Springer-Verlag, 2007.
6. Westerweel J., "Efficient detection of spurious vectors in particle image velocimetry data", *Experiments in Fluids*, **16**(3), 1994.
7. Miller, D.R., Comings, E.W., "Force momentum fields in a dual-jet flow", *Journal of Fluid Mechanics* **7**, pp. 237–256, 1960.
8. Tanaka, E., "The interference of two-dimensional parallel jets (1st report, experiments on dual jet)". *Bulletin JSME* **13**, pp. 272–280, (1970).
9. Tanaka, E., "The interference of two-dimensional parallel jets (2nd report, experiments on the combined flow of dual jet)". *Bulletin JSME* **17**, pp. 920–927, 1974.
10. Ko, NWM and Lau, KK, "Flow structures in initial region of two interacting parallel plane jets", *Experimental Thermal and Fluid Science*, **2**(4), 1989.
11. Lin, YF and Sheu, MJ, "Investigation of two plane paralleltiinven ilated jets", *Experiments in Fluids*, **10**(1), 1990.
12. Nasr, A and Lai, JCS, "Comparison of flow characteristics in the near field of two parallel plane jets and an offset plane jet", *Physics of Fluids*, **9**(10), 1997.
13. Durve, A and Patwardhan, A. W and Banarjee, I and Padmakumar, G and Vaidyanathan, G, "Numerical investigation of mixing in parallel jets", *Nuclear Engineering and Design*, **242**, 2012.
14. Namer, I and Ötügen, MV, "Velocity measurements in a plane turbulent air jet at moderate Reynolds numbers", *Experiments in Fluids*, **6**(6), 1998.
15. H.-M Prasser, A Böttger, J Zschau, A new electrode-mesh tomograph for gas–liquid flows, Flow Measurement and Instrumentation, **9**(2), 1998, pp. 111-119.